JACS
JOURNAL OF THE AMERICAN CHEMICAL SOCIETY

ARTICLE

pubs.acs.org/JACS

Hybrid Heterojunction Solar Cell Based on Organic−Inorganic Silicon Nanowire Array Architecture

Xiaojuan Shen,[†] Baoquan Sun,*[,†] Dong Liu,[†] and Shuit-Tong Lee*[,‡]

[†]Jiangsu Key Laboratory for Carbon-Based Functional Materials & Devices, Institute of Functional Nano & Soft Materials (FUNSOM), Soochow University, 199 Ren'ai Road, Suzhou 215123, China

[‡]Center of Super-Diamond and Advanced Films (COSDAF) and Department of Physics and Materials Science, City University of Hong Kong, Hong Kong SAR

Supporting Information

ABSTRACT: Silicon nanowire arrays (SiNWs) on a planar silicon wafer can be fabricated by a simple metal-assisted wet chemical etching method. They can offer an excellent light harvesting capability through light scattering and trapping. In this work, we demonstrated that the organic−inorganic solar cell based on hybrid composites of conjugated molecules and SiNWs on a planar substrate yielded an excellent power conversion efficiency (PCE) of 9.70%. The high efficiency was ascribed to two aspects: one was the improvement of the light absorption by SiNWs structure on the planar components; the other was the enhancement of charge extraction efficiency, resulting from the novel top contact by forming a thin organic layer shell around the individual silicon nanowire. On the contrary, the sole planar junction solar cell only exhibited a PCE of 6.01%, due to the lower light trapping capability and the less hole extraction efficiency. It indicated that both the SiNWs structure and the thin organic layer top contact were critical to achieve a high performance organic/silicon solar cell.

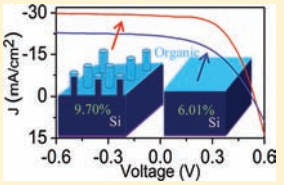

INTRODUCTION

There is a great interest to develop photovoltaic structures made from low-cost materials and simple fabrication processes.[1] Silicon nanowire arrays (SiNWs), which can enhance the light path length by up to a factor of 73 in comparison with that of bulk silicon, can act as a light trapping layer.[2] Thus, using this structure, it may allow cell fabrication with less silicon materials and save the cost. Nowadays, the p−n junction architectures composed of vertical SiNWs have been widely explored.[2−17] On the basis of such geometry, n-type SiNWs were deposited by p-type amorphous Si (a-Si) and subsequently crystallized with high temperature annealing.[4,18] The p−n homojunction could also be formed via ion implantation and subsequent rapid thermal annealing to activate the dopants.[7] The cells showed performance in SiNWs structures superior to that in the planar ones. However, these inorganic geometry cells composed of p−n junctions required a series of complicated fabrication process, and some steps even had to be done at high temperatures (up to 1000 °C). The best resulting photovoltaic devices showed a promising power conversion efficiency (PCE) of 11%.[19] Alternatively, conjugated polymers including poly(3,4-ethylene dioxythiophene):poly(styrenesulfonate) (PEDOT:PSS) or poly(3-hexylthiphene) combined with silicon nanostructure were used to fabricate the organic−inorganic hybrid device.[20−25] Because organic conjugated molecules can be processed by wet chemical method at low temperature, it is possible to fabricate hybrid solar cells based on SiNWs and conjugated polymer with a simple fabrication process as a technological alternative.[26,27] However, the hybrid devices only displayed moderate PCE of 5−6%.[20−22,28,29] To our best knowledge, there is no report on realizing the importance of the structure of a thin organic layer around the SiNWs on the planar component to achieve an efficient device, because the size of most conjugated polymers is too big to filtrate into the bottom space of the adjacent wires and form a thin layer around the SiNWs. In this study, we used a small conjugated molecule as the hole transport layer. The organic semiconductor of 2,2,7,7′-tetrakis(*N*,*N*-di-*p*-methoxyphenyl-amine)-9,9′-spirobifluorene (spiro-OMeTAD) was deposited onto SiNWs standing on a planar silicon wafer by the solution processing method. Using a simple processing technique, the hybrid solid-state inorganic−organic heterojunction on the planar component devices achieved a PCE of ∼9.70%, which was ascribed to the enhancement of the light absorption and the improvement of the charge-carrier extraction efficiency. In this hybrid solar cell, the single crystal silicon substrate played a primary role in the achievement of the high performance device. However, the sole planar junction solar cell only exhibited a PCE of 6.01% due to the less hole extraction efficiency and lower light trapping capability. We demonstrated that both the SiNWs structure and the thin organic layer top contact were critical to achieve a high performance organic/silicon solar cell.

EXPERIMENTAL SECTION

SiNWs Preparation. SiNWs on the planar silicon substrate is made using a previously reported method by metal ion-assisted aqueous

Received: July 9, 2011
Published: October 28, 2011

Scheme 1. (a) Chemical Structures of Spiro-OMeTAD and PEDOT:PSS; (b) SiNWs Solar Cell with Core−Shell Architectures, Schematic Cross-Section View of the Inorganic Silicon Nanowire as Core on Bulk Silicon Substrate (Deep Blue) and Organic Spiro-OMeTAD as Shell (Light Blue); and (c) SiNWs Solar Cell with Embedded Architectures, Schematic Cross-Section View of the Embedded Structure with SiNWs on Bulk Silicon Substrate (Deep Blue) Embedded in Spiro-OMeTAD (Light Blue)[a]

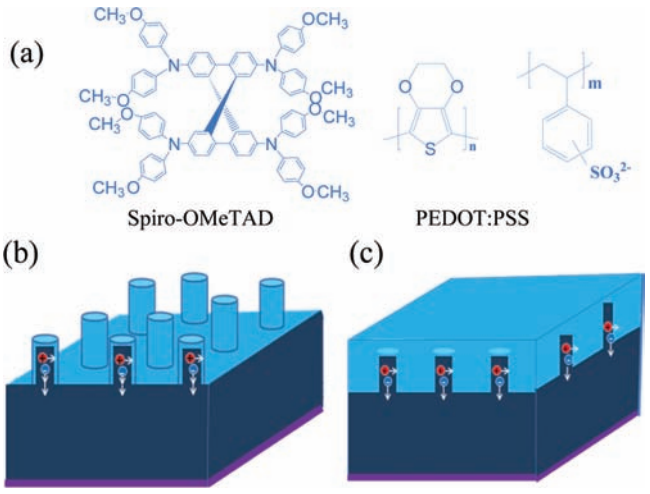

[a] The bottom purple layer stands for In/Ga alloy. The different parts of the scheme did not stand for the layer thickness of the real devices. In the real devices, the silicon part was much thicker than that of the length of SiNWs.

electroless etching.[11] In brief, clean n-type Si (100) substrates (resistivity of ∼5 Ω cm) were immersed in an aqueous solution of HF (4.8 M) and $AgNO_3$ (0.02 M) for 15 min at the room temperature. The substrates were dipped into the aqueous solution of HNO_3 (30% W/W) and then rinsed with deionized (DI) water to remove any residual silver. Silicon oxide was removed by wet chemical etching in aqueous HF (5 M) with gentle shaking for 10 min. Next, they were immersed in DI water and dried under a stream of nitrogen gas. The hydrogen-terminated silicon (H−Si) was obtained in this step. The H−Si substrates were immediately taken into the glovebox.

Methylation Process. Methyl group-terminated (CH_3−Si) substrates were prepared following a two-step chlorination/alkylation method.[30−34] First, H−Si substrates were dipped into a saturated solution of PCl_5 in chlorobenzene (CB) at 90 ± 10 °C under inert atmosphere to terminate the silicon surface with a chlorinated group (Si−Cl). The Si−Cl samples were then rinsed sequentially with CB and tetrahydrofuran (THF) three times. Next, the Si−Cl substrates were subsequently dipped into a solution of CH_3MgCl (1 M) in THF for at least 8 h at 70 ± 10 °C and then rinsed with THF and methanol. The samples were taken out of the glovebox, immersed in DI water for 10 min, and then rinsed sequentially with acetone and ethanol.

SiNWs Characterization. The morphology of SiNWs on the planar silicon substrate was carried out with a FEI Quanta 200 FEG high-resolution scanning electron microscope (SEM). A FEI Tecnai G2 F20 STWIN transmission electron microscope (TEM) was used to characterize SiNWs coated with spiro-OMeTAD. Reflectance spectra were characterized by a Perkin-Elmer Lambda-750 using LABSPHERE reflectance integrating spheres. Absorption spectra were measured from solid films on quartz substrates. X-ray photoelectron spectroscopy (XPS) was performed with a KRATOS-AXIS-DLD spectrometer using a monochromatic Al Kα source (1486.6 eV).

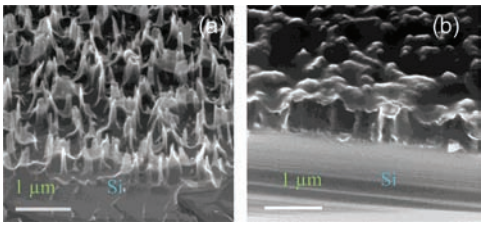

Figure 1. (a) Cross-section SEM image of device 1 corresponding to Scheme 1b with the core−shell structure. (b) Cross-section SEM micrograph of device 3 corresponding to Scheme 1c with the embedded structure.

Device Fabrication. The SiNWs were coated with spiro-OMeTAD (chemical structure shown in Scheme 1a) as the hole transport layer to form a core−shell structure (Scheme 1b) or embedded structure (Scheme 1c) on the planar component by controlling the thickness of the organic layer. First, spiro-OMeTAD was dissolved in CB at 70 °C for 30 min. Second, lithium bis(trifluoromethylsulfonyl)imide salt (Li-TSFI), predissolved in acetonitrile, was added to the spiro-OMeTAD solution. Finally, the mixed spiro-OMeTAD solution was deposited onto the entire surface of the SiNWs electrodes for a few tens of seconds before the spin-coating process. The thickness of the organic layer was controlled by the concentration of spiro-OMeTAD as well as the spin-coating velocity and times. In some devices, a thin layer of PEDOT:PSS (chemical structure depicted in Scheme 1a) was deposited onto the top of spiro-OMeTAD. Next, hybrid substrates were finally loaded under vacuum for thermal evaporation of copper or silver electrodes. Back ohmic contacts were obtained by first etching the rear side of silicon surface in diluted HF (aq), depositing a thin layer of In:Ga eutectic onto the freshly etched surface, and then mounting each sample on an aluminum support.

Device Characterization. The photovoltaic characterization was conducted in an ambient environment. Newport 91160 solar simulator equipped with a 300 W xenon lamp and an air mass (AM) 1.5 filter was used to generate simulated AM 1.5 solar spectrum irradiation source. The irradiation intensity was 100 mW/cm^2 calibrated by a Newport standard silicon solar cell 91150. Newport monochromator 74125 and power meter 1918 with silicon detector 918D were used in the external quantum efficiency (EQE) measurements. All of the electrical data were recorded by a Keithley 2612 source meter. The capacitance was characterized with a Wayne Kerr 6500B impedance analyzer.

RESULTS AND DISCUSSION

Hybrid Heterojunction with SiNWs on the Silicon Substrate. The core−shell structure with SiNWs on a planar silicon substrate can be used to enhance the light harvesting capability and improve the carrier collection efficiency. Here, SiNWs acted as the core, while spiro-OMeTAD was deposited by the spin-coating process forming a sheath and acting as the hole transport layer. The diameter of SiNW was ∼20−100 nm, and the density was ∼10^8−10^9/cm^2. Spiro-OMeTAD is a p-type organic semiconductor and widely used as the hole transport layer in the solid-state dye-sensitized solar cell, yielding the highest efficiency of 5.1%.[35−38] There are several advantages in using spiro-OMeTAD. First, spiro-OMeTAD is an organic noncrystalline molecule with high glass-transition temperature. Crystallization is undesirable because it would impair the formation of a good contact between SiNWs and the hole conductor. Second, spiro-OMeTAD is a small molecule. Its small size ensures better solubility in organic solvents, benefiting it easily to arrive at the bottom part of SiNWs.[38,39] Third, as compared to the previously

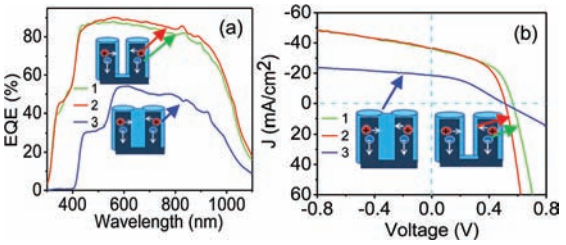

Figure 2. Output characteristics of hybrid devices with different device structures. (a) EQE spectra of device 1 (In:Ga/SiNWs/spiro-OMeTAD/PEDOT:PSS/Cu (core−shell)), device 2 (In:Ga/SiNWs/spiro-OMeTAD/Cu (core−shell)), and device 3 (In:Ga/SiNWs/spiro-OMeTAD/Cu (embedded structure)). (b) Current density−voltage behavior of devices 1, 2, and 3 under simulated AM 1.5 solar irradiation at 100 mW/cm^2. The inset images stand for the structures of the devices.

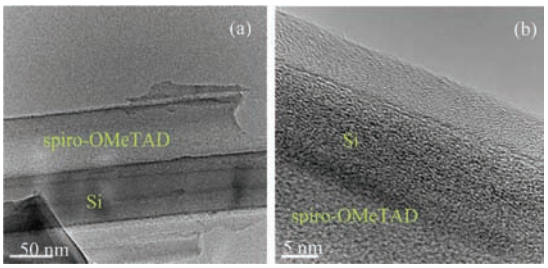

Figure 3. (a) TEM image of single wire displaying silicon core and organic shell. (b) High-resolution TEM image of single wire showing an interface of inorganic (crystallized phase) and organic (amorphous one).

reported a-Si (band gap of ∼1.7 eV) as the sheath,[4] spiro-OMeTAD displays a relatively narrower light absorption range and lower absorption coefficient (Figure S1), which ensures that more light can reach SiNWs. However, it exhibits a low hole mobility of ∼10^{-3}−10^{-4} cm^2 V^{-1} s^{-1}. Thus, a thin layer of spiro-OMeTAD is essential for both efficient charge collection and less light filter effect. Figure 1a displayed a cross-section SEM image of a device with n−p inorganic−organic core−shell architecture (Scheme 1b) after deposition of spiro-OMeTAD onto SiNWs. To verify the necessity of a thin organic layer, a thick layer was deposited onto SiNWs for comparison, where SiNWs on the planar silicon wafer were completely embedded in the organic layer (Scheme 1c). The SEM image of the corresponding embedded structure was shown in Figure 1b. In addition, a conducting polymer of PEDOT:PSS was inserted between the spiro-OMeTAD layer and anode to improve the collection properties of the interface.[40] Here, to simplify the structure description, devices 1, 2, and 3 were defined as having the architectures of In:Ga/SiNWs/spiro-OMeTAD/PEDOT:PSS/Cu (core−shell), In:Ga/SiNWs/spiro-OMeTAD/Cu (core−shell), and In:Ga/SiNWs/spiro-OMeTAD/Cu (embedded structure), respectively, where SiNWs stood for the wire arrays standing on the planar silicon substrate. The schematic structure and real device image for devices 1, 2, and 3 were illustrated in Figure S2.

High carrier transfer and collection efficiency are necessary to achieve a large EQE value. The EQE spectra of devices 1 and 2 as shown in Figure 2a indicated that the carrier transfer and collection should be rather efficient in the present inorganic−organic core−shell structure.[36] In addition, the high EQE value also stemmed from the respectable charge properties of the thin

Table 1. Response of Hybrid Solar Cells with Different Device Structures under Simulated AM 1.5 Solar Irradiation at 100 mW/cm^2

device	V_{oc} (V)	integrated J_{sc} (mA/cm^2)	FF	PCE (%)
1[a]	0.568	32.5	0.504	9.30
2[b]	0.512	33.7	0.500	8.63
3[c]	0.504	16.7	0.371	3.12

[a] Device 1 (In:Ga/SiNWs/spiro-OMeTAD/PEDOT:PSS/Cu (core−shell)). [b] Device 2 (In:Ga/SiNWs/spiro-OMeTAD/Cu (core−shell)). [c] Device 3(In:Ga/SiNWs/spiro-OMeTAD/Cu (embedded structure)). Here, SiNWs stands for SiNWs standing on a planar silicon substrate.

spiro-OMeTAD layer.[35] Here, the EQE was measured in an area within 1 mm of the copper electrode due to the extra absorption from the top electrodes as shown in Figure S3. Devices 1 and 2 displayed a wide spectrum response range of 300−1100 nm and large EQE values of ∼90% at their peaks. The profile was similar to that of the traditional silicon solar cell.[41] The TEM image of a single silicon nanowire was shown in Figure 3a, where the silicon was covered with a thin organic layer (∼50 nm). In the high-resolution TEM image in Figure 3b, it was clear to see that there was an amorphous layer covering the crystallized silicon nanowire surface. In comparison, device 3 presented a narrower spectrum range due to the strong absorption of the thick spiro-OMeTAD film below 400 nm as well as a lower peak EQE value of ∼54%. As compared to the short distance of the core−shell structure, the moderate EQE value was ascribed to the inefficient hole collection efficiency in the long-distance transport process from the interface to the top electrode. It illustrated that a thin organic layer benefited the higher efficiency of hole collection. Figure 2b showed electrical output characteristics of the current density versus voltage (J−V), and their parameters were summarized in Table 1. Under simulated AM 1.5 solar irradiation at 100 mW/cm^2, device 1 displayed an open-circuit voltage (V_{oc}) of 0.568 V, a short-circuit current density (J_{sc}) of 36.0 mA/cm^2, and a fill factor (FF) of 0.504. Here, only the active area of the top electrode contact (as shown in Figure S2) was used to determine the J_{sc}. However, the PEDOT:PSS top contact is also somewhat conductive; thus, the current may be collected from areas not directly in contact with the electrode. Furthermore, minority carriers can diffuse a certain distance in silicon, so the light absorbed by silicon away from the top electrode contact may also contribute to the photocurrent. In that way, we used a method to roughly evaluate the PCEs of devices 1, 2, and 3 only for comparative purpose, calibrating the J_{sc} from the integrated EQE value. This method was also used in a similar organic−inorganic device.[21] The EQE value was measured very closely to the electrode by a focused spot, as shown in Figure S3. Because the size of the light spot was smaller (∼1 mm × 1 mm) than both the measured device and the calibrated diode, the uncertain active area should be avoided. Using a solar photon flux of standard AM 1.5 spectrum, a simple multiplication with the EQE spectrum and the elementary charge will lead to a calculated J_{sc}. Thereafter, we used the integrated J_{sc} value to calibrate the measured one. By integration from 280 to 1100 nm, a J_{sc} of 32.5 mA/cm^2 was obtained for device 1, which was ∼10% different from a directly measured value of 36.0 mA/cm^2. We corrected the J_{sc} according to the integrated one, and the estimated PCE for this type of structure was around 9.3%. This value was only used to compare

the performance of devices 1, 2, and 3. An alternative method to determine the PCE will be discussed as follows.

Heterojunction with core−shell structure SiNWs on the planar silicon, where suspending silicon bonds were terminated with methyl group, was crucial for an enhancement of the device performance. Alkylation of crystalline silicon was displayed to offer minimal surface recombination.[30,33,34,42] The surface recombination velocity of such surfaces can be as low as 45 cm/s,[43] decreasing the probability of electron−hole recombination. Thus, the carrier collections of silicon nanowire will be increased.[30] In our experiment, a two-step chlorination/alkylation method was used to terminate the silicon surface with a methyl group.[31−34] Figure S4 displayed the C1s XPS emission region of CH_3−SiNWs, fitted to three peaks: C−Si, C−C, and C−O. The C−Si peak was attributed to the methyl group chemically bonded to the Si surface. The C−C and C−O peaks were assigned to adventitious hydrocarbons containing oxygen that were physically bonded to either hydrogen or carbon atoms of the methyl group on the silicon surface. This observation was consistent with that of a previous report.[33] The following soft solution-processable fabrication can retain the organic layer. This ultrathin organic monolayer can dramatically suppress charge recombination, leading to an enhancement of the photovoltaic device. On the contrary, the hybrid device based on H−SiNWs only gave a weak photoresponse, as shown in Figure S5, which was different from those of previous organic−silicon hybrid devices.[20−22,28,44] We believed that the difference resulted from the interface variation. The poor performance could be ascribed to large surface recombination velocity and an unsuitable band alignment.[23] In previous reports, there would always be a thin oxidation layer on the silicon surface when it was exposed to air.[20,21] The oxidation layer could also retard the charge recombination at the organic−inorganic interface.[45] In addition, a surface-current-induced oxidation had been developed to verify that the oxidation layer could enhance the performance of organic−inorganic device.[44] However, the surface of the H−SiNWs in our experiments was carefully controlled through immediately transferring the substrate into a glovebox.

Device 2 displayed a V_{oc} of 0.512 V, an integrated J_{sc} of 33.7 mA/cm^2, and a FF of 0.500 for an overall estimated PCE of 8.6% in the absence of PEDOT:PSS layer. The FF and the J_{sc} in device 2 were similar to those in device 1. However, the V_{oc} decreased in the absence of the PEDOT:PSS layer. The presence of the PEDOT:PSS layer is advantageous to the higher V_{oc}, which may be due to the improved organic/inorganic interface.[40] As shown in previous reports, the injection/collection properties of the silicon/PEDOT:PSS interface were superior to those of the silicon/metal one.[46] The velocity of majority carrier charge transfer is several orders of magnitude larger at the Si/Au junctions than that at the Si/PEDOT:PSS contacts, resulting in superior photoresponse characteristics for the inorganic/organic interface. Here, pinhole area still coexisted on the surface of silicon after deposition of the thin layer of spiro-OMeTAD. These pinholes would cause the metal to directly contact with silicon, leading to a higher leakage current. As compared to the dark current level of devices 1 and 2, as shown in Figure S6, the absence of PEDOT:PSS layer displayed a larger leakage current level, resulting in a lower V_{oc}.[47] Device 3 yielded a V_{oc} of 0.504 V, an integrated J_{sc} of 16.7 mA/cm^2, and a FF of 0.370 for an overall estimated PCE of 3.1% when SiNWs were embedded in spiro-OMeTAD. This moderate performance was similar to that of previously reported SiNWs/conjugated polymer. The poor device performance should be related to the lower efficiency of hole transport.[3,20,28]

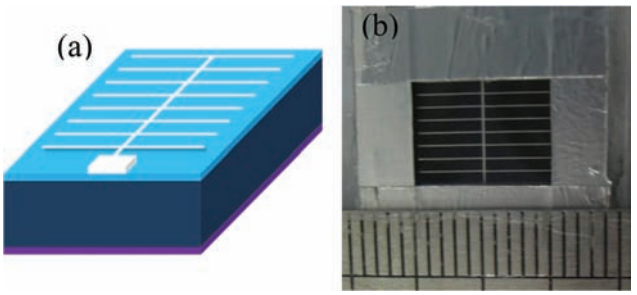

Figure 4. (a) Schematic structure of the device with top grid electrodes. The silicon substrate (deep blue) is covered with the organic layer (light blue). The top was the grid Cu:Ag electrode (white), and the rear metal was In:Ga (purple). (b) The real image of the device with top grid electrodes. The area where there was no grid electrode was covered with opaque aluminum foil. The region where light was illuminated was 1.0 cm × 0.8 cm.

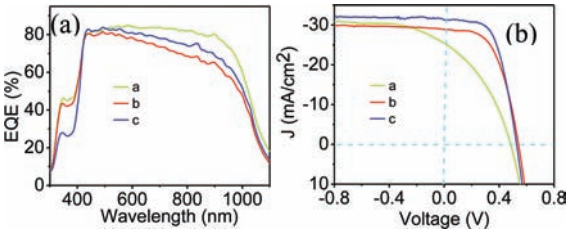

Figure 5. Output characteristics of hybrid devices with different top contacts. All of the devices were in a core−shell structure and with top grid metal Cu(50 nm): Ag(100 nm) electrodes. (a) EQE spectra of device a, (In:Ga/SiNWs/spiro-OMeTAD/Cu:Ag), where PEDOT:PSS was not inserted before the deposition of grid electrodes; device b, (In:Ga/SiNWs/spiro-OMeTAD/PEDOT:PSS/Cu:Ag), where PEDOT:PSS was spin-cast on the top of spiro-OMeTAD before deposition of the grid Cu:Ag electrodes; and device c, (In:Ga/SiNWs/spiro-OMeTAD/Cu/PEDOT:PSS/Cu:Ag, where both 2 nm-thick Cu and PEDOT:PSS were deposited onto the whole layer of spiro-OMeTAD in sequence before deposition of the grid electrodes. (b) Current density−voltage behavior of devices a, b, and c under simulated AM 1.5 solar irradiation at 100 mW/cm^2.

As discussed above, the J_{sc} could be overestimated because the minority carriers generated by the silicon away from the top metal electrode could also be collected by the electrodes. In that case, the grid shape electrode was used as the top contact, and the structure scheme and real device image are shown in Figure 4a and b, respectively. To avoid the extra charge collecting out of the grid shape region, opaque aluminum foil was used to cover the region away from the electrode. Therefore, only the region with the metal grid electrode was illuminated with the light. In the following part, all of the devices were fabricated by depositing the grid electrodes except for the exceptional case mentioned. On the basis of the grid electrodes, the best hybrid inorganic−organic core−shell device attained a PCE of 9.70%, which will be discussed below. This value was higher than the previously reported efficiency for SiNWs cell with inorganic−organic core−shell structure.[2,4,5,7,9,11]

Top Contact Effect. The top contact displayed a critical role on the hole collecting efficiency of the devices. As discussed in the previous section, PEDOT:PSS acted as a buffer layer between

Table 2. Response of Hybrid Solar Cells with Different Top Contacts under Simulated AM 1.5 Solar Irradiation at 100 mW/cm^2

device	V_{oc} (V)	J_{sc} (mA/cm^2)	FF	PCE (%)
a[a]	0.484	25.5	0.365	4.50
b[b]	0.542	28.9	0.541	8.47
c[c]	0.527	31.3	0.588	9.70

[a] (In:Ga/SiNWs/spiro-OMeTAD/Cu:Ag), where PEDOT:PSS was not inserted before the deposition of grid electrodes. [b] (In:Ga/SiNWs/spiro-OMeTAD/PEDOT:PSS/Cu:Ag), where PEDOT:PSS was spin-cast on the top of spiro-OMeTAD before deposition of the grid Cu:Ag electrodes. [c] (In:Ga/SiNWs/spiro-OMeTAD/Cu/PEDOT:PSS/Cu:Ag), where both 2 nm-thick Cu and PEDOT:PSS were deposited onto the whole layer of spiro-OMeTAD in sequence before deposition of the grid electrodes. Here, SiNWs stands for SiNWs standing on a planar silicon substrate.

spiro-OMeTAD and copper to improve the contact property. In addition, for the devices with grid top electrodes, transparent PEDOT:PSS also played a charge collecting role because the holes in the spiro-OMeTAD layer could not be efficiently collected due to its inferior hole mobility. As shown in Figure 5b, the device with spiro-OMeTAD directly in contact with Cu grid electrodes displayed a V_{oc} of 0.484 V, a J_{sc} of 25.5 mA/cm^2, and a FF of 0.365, which yielded a modest PCE of 4.51%. On the contrary, an additional layer of PEDOT:PSS between spiro-OMeTAD and top grid electrodes resulted in a dramatic enhancement of device performance. The device with the PEDOT:PSS layer exhibited a V_{oc} of 0.542 V, a J_{sc} of 28.9 mA/cm^2, and a FF of 0.541, generating a PCE of 8.47%. The higher V_{oc} could be ascribed to the prohibition of the formation of shunt path in the metal deposition process when PEDOT:PSS was present. This observation was consistent with the above observation, as shown in Figure 2. In addition, both the J_{sc} and the FF were improved. In this case, the enhancement of device performance in the presence of PEDOT:PSS could be attributed to two factors: improvement of the electrode contact and enhancement of the hole collection efficiency. In the traditional silicon solar cell with grid electrodes, especially for the amorphous silicon as the passivation and hole collection layer, high conductivity and transparent indium tin oxide (ITO) was deposited between silicon and the top grid electrodes to improve the charge collection efficiency.[47] Unfortunately, our hybrid device with radio frequency sputtered ITO electrode as transparent electrodes combined with the grid metal electrodes displayed an inferior device performance. We believed that the polymer film could be partly damaged in the sputtering process, which resulted in poor performance. Fortunately, we found that a very thin layer of copper (~2 nm) by thermal evaporation could enhance the J_{sc} and the FF before depositing PEDOT:PSS onto spiro-OMeTAD. As shown in Figure 5, the device with an extra ~2 nm-thick copper achieved a V_{oc} of 0.527 V, a J_{sc} of 31.3 mA/cm^2, and a FF of 0.588, which yielded the PCE of 9.70%. Obviously, both the J_{sc} and the FF were further improved in the presence of the ultrathin copper layer. We conceived that the improvement should be ascribed to an enhancement of the hole collection efficiency. However, the V_{oc} was slightly decreased due to the possible formation of shunt path, which was similar to that in the previous case. The electrical output characteristics of the devices with different top contacts were summarized in Table 2. However, in the present case, the conductivity of PEDOT:PSS was still far below that of ITO. Therefore, it is believed that modest charge transport properties of transparent electrode should still be a limiting factor for the J_{sc} and the FF.

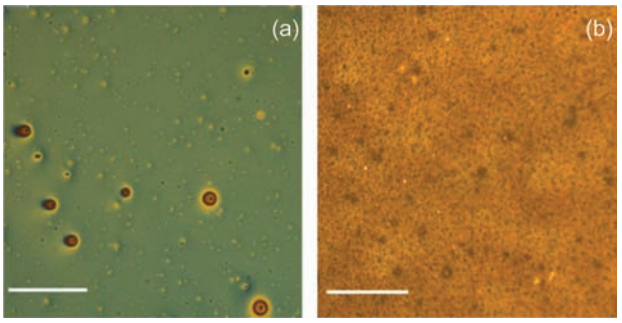

Figure 6. Optical microscopy images of spiro-OMeTAD film on (a) flat silicon and (b) SiNWs. The films were fabricated by the same spin-coating process with spiro-OMeTAD concentration of 13 mg/mL. The scale bars are 500 μm.

It is worth pointing out that all of the EQE values were similar in the cases of the devices with or without PEDOT:PSS layer insertion (as shown in Figures 2a and 5a). However, using the grid top electrode, the J_{sc} displayed different values when the devices were characterized under AM 1.5 solar illumination at 100 mW/cm^2 (as shown in Figure 5b). The difference should originate from the charge collection capability of the spiro-OMeTAD layer under various light illumination. Generally, the EQE was measured under weak light illumination at a single wavelength (typical intensity at several mW/cm^2), and our measurement was done like this. The generated charges could be efficiently collected solely by the spiro-OMeTAD layer at low light intensity illumination because they were in the range of the collection capability of spiro-OMeTAD layer. However, the PCE was characterized at high light intensity illumination, where intensity was 10−100 times stronger than that where EQE was measured. The amount of generated charges was too large to be transported efficiently only by spiro-OMeTAD. Therefore, charges could be piled up and led to serious charge recombination. In that case, the PEDOT:PSS layer was indispensable to efficiently transport the generated charge to the metal electrodes at high light intensity illumination. The higher conductivity of PEDOT:PSS is deposited, and less charge will be piled up away from the metal electrodes. On the contrary, this case was not observed if the top transparent electrode was used as the active layer, as shown in Figure 2b, which further verified the necessity of PEDOT:PSS layer. However, the near-infrared EQE spectrum decreased slightly when the PEDOT:PSS layer was inserted, which could be ascribed to the weak absorption of the PEDOT:PSS layer in this spectral range.

Planar Junction. The sole planar silicon substrate was also used for hybrid device to verify the necessity of SiNWs with thin organic layer on the planar component to achieve the high efficiency organic−inorganic hybrid solar cell. However, reducing the thickness of the organic layer was limited by technology problems if we wanted to deposit a continuous spiro-OMeTAD layer without generating shunt paths in the subsequent process steps. Because the silicon surface anchored with methyl group was too hydrophobic to allow spiro-OMeTAD to be adhered, the thin liquid layer would shrink quickly during the spin coating process. As is shown in Figure 6a, there were many spots formed on the polished CH_3−Si surface after spiro-OMeTAD deposition.

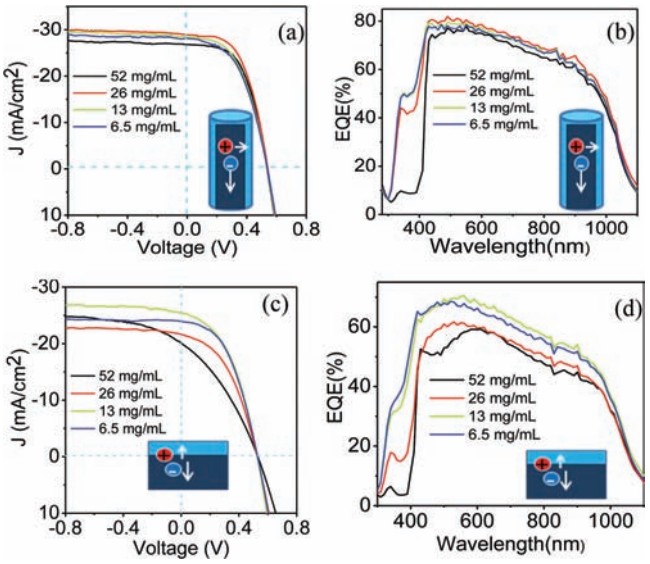

Figure 7. Output characteristics of hybrid devices. (a) Current density−voltage behavior and (b) EQE spectra of SiNWs heterojunction with different thicknesses of spiro-OMeTAD layer. (c) Current density−voltage behavior and (d) EQE spectra of planar silicon junction with different thicknesses of spiro-OMeTAD layer. The inset images display the junction types.

Table 3. Response of Hybrid Solar Cells Based on Planar Silicon or SiNWs Junction with Different Thicknesses of Spiro-OMeTAD under Simulated AM 1.5 Solar Irradiation at 100 mW/cm^2

junction type	conc[a] (mg/mL)	V_{oc} (V)	J_{sc} (mA/cm^2)	FF	PCE (%)
planar Si	52	0.531	20.2	0.336	3.60
	26	0.526	21.7	0.438	5.19
	13	0.527	25.5	0.447	6.01
	6.5	0.529	24.0	0.466	5.91
SiNWs on Si	52	0.537	26.8	0.552	7.94
	26	0.542	28.9	0.541	8.47
	13	0.538	28.2	0.508	7.71
	6.5	0.538	28.1	0.495	7.48

[a] Concentration of spiro-OMeTAD in chlorobenzene solvent.

On the contrary, the methylated SiNWs substrate surface displayed a uniform film when being coated with spiro-OMeTAD, as illustrated in Figure 6b. The presence of pinhole would result in the metal directly in contact with silicon as discussed above. In that case, a thick layer of spiro-OMeTAD for planar junction had to be utilized to avoid pinhole formation. However, a thick organic layer could reduce the charge collection efficiency. To obtain the optimum thickness of organic layer, spiro-OMeTAD solutions with different concentration were spin-casted onto a planar silicon substrate. The $J-V$ curves illuminated under standard solar irradiation and EQE spectra of the devices based on sole planar silicon junction were illustrated in Figure 7c and d. Their electrical output characteristics were summarized in Table 3. As expected, the performance of the planar junction devices could be enhanced with increasing thickness of spiro-OMeTAD layer. The best device with planar junction displayed a V_{oc} of 0.527 V, a J_{sc} of 25.5 mA/cm^2, and a FF of 0.447, which yielded a modest PCE of 6.01%.

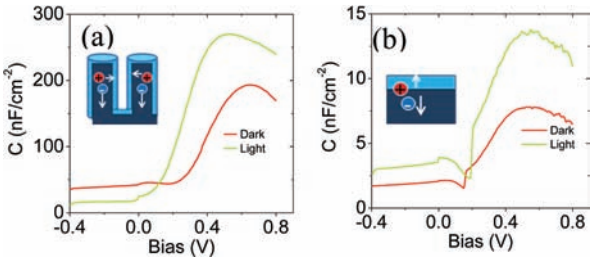

Figure 8. Experimental C−V data measured on the devices with different structures under both dark and light. The insets show the schematics of the devices representing different kinds of junction structures: (a) heterojunction based on SiNWs on silicon substrate with core−shell structure; and (b) sole planar silicon junction.

Comparison between SiNWs on the Silicon Substrate and the Sole Planar Substrate. For comparison, the same concentration of spiro-OMeTAD was also deposited onto SiNWs to obtain heterojunction architecture. The $J-V$ curves illuminated under standard solar irradiation and EQE spectra of the heterojunction were plotted in Figure 7a and b. The electrical output characteristics of the heterojunction were summarized in Table 2. All of the heterojunction devices with SiNWs on the silicon substrate displayed superior performances over those of the sole planar substrates. The J_{sc} was dramatically enhanced in the SiNWs heterojunction, mainly due to the improved light harvesting capability. The dramatically suppressed light reflection of SiNWs on the planar silicon was shown in Figure S7. However, the V_{oc} values were quite similar. Generally, the higher V_{oc} would be expected from an increase in the J_{sc} arising from the heterojunction architecture. Meanwhile, the increased V_{oc} would also be offset by the larger interface.[7,48] The combined effects led to the similar V_{oc} values. In addition, the efficiency was deteriorated with increasing thickness of spiro-OMeTAD in the core−shell structure junction. The lower efficiency could be ascribed to the inefficient carrier collection properties for the thicker spiro-OMeTAD layer.

The superior efficiency of the devices based on the heterojunction with SiNWs on the planar silicon should be ascribed to the excellent light harvesting properties as well as efficient carrier collection efficiency both from the wires and from the planar components. First, the additional light harvesting from multiple reflections within the wire array structure can contribute to the higher J_{sc}. The optimum heterojunction device based on core−shell SiNWs on the planar silicon substrate exhibited about 1.3 times higher J_{sc} than that of the sole planar junction cell. Second, the substrate of SiNWs on the planar silicon wafer presents a better uniform film when coated with spiro-OMeTAD, forming a good contact interface between the silicon/organic and organic/electrode. In addition, the FF for the heterojunction devices always displayed a higher value than those of the planar ones. Therefore, the enhancement in the SiNWs heterojunction cannot be explained solely on the basis of enhanced light absorption.

The heterojunction based on SiNWs on the silicon substrate could provide more junction area to allow efficient charge-carrier separation and extraction, which was determined by capacitance measurement.[16] Capacitances of the devices with sole planar junction and one with core−shell SiNWs on the planar silicon structure were measured at room temperature under both dark and illumination conditions, as shown in Figure 8, to evaluate the

junction area of organic/inorganic heterojunction. The capacitances of the devices reached the maximum near V_{oc} region when the depletion layer was very thin driven by the forward electric field between anode and cathode, and thus the capacitance value at this point could indicate the junction area of devices. The capacitance was measured against different bias voltage, with an AC excitation amplitude of 100 mV at a frequency of 1 kHz. The capacitance shown was per unit base-area (not junction area). One can differentiate the $C-V$ bias range into two different regions, smaller than the V_{oc} (around 0.55 V) and larger than the V_{oc}. In the dark environment, the capacitances of both devices remained nearly constant until the applied bias is close to V_{oc}. The maximum capacitance of sole planar device under dark was $\sim$7.5 nF cm^{-2} at the forward bias of $\sim$0.5−0.6 V, whereas that of the core−shell structure reached 190 nF cm^{-2} in the similar bias range. The $\sim$25 times capacitance increase in core−shell structure on the planar silicon device indicated a huge increasing junction area as compared to that of the sole planar one. In addition, the hybrid junction with SiNWs on silicon substrate provided more depletion region to allow efficient charge separation.[16] The SiNWs junction devices showed a $\sim$40% increase in the capacitance at the voltage range between negative bias to the V_{oc} under illumination. It indicated that the photogenerated charges could still be relatively efficiently collected by the electrode and a small amount of charge accumulation occurred. However, for the planar junction device, a significant increase ($\sim$75%) was observed in the same bias range, which implied the photogenerated carriers were piled up within the heterojunction region and could not be extracted by the electrode effectively. By comparing the $C-V$ measurement results, we conceived that the imbalanced mobility in the planar junction device would cause charge accumulation within the device, which resulted in the lower FF and J_{sc} in the sole planar junction device, as shown in Table 3. Considering these factors, it could be understood why the planar silicon/spiro-OMeTAD heterojunction displayed the inferior performance as compared to the three-dimensional structure.

On the basis of our own experiences, the hybrid heterojunction consisting of SiNWs on the planar silicon in combination with efficient surface passivation would be the key factor to achieve the high performance hybrid solar cell. At present, although the heterojunction solar cell with core−shell structure on the planar silicon substrate displayed a superior J_{sc}, the cell efficiency was still less than that of bulk p−n homojunction crystalline silicon solar cells,[41] resulting from the moderate V_{oc} and FF. The p−n heterojunction as charge-segregation region in photovoltaics implies the drawback of possible defect states, causing high surface recombination losses as an additional and possibly dominating path at the heterojunction. In our preliminary simulation, the density of state of the organic−inorganic interface might be the main factor taking the responsibility for the lower values of the V_{oc} and FF. The lower interface density of state would lead to the higher V_{oc} as well as the improved FF. On the contrary, it displayed the neglectable effects on the J_{sc} when it varies from 10^{10} to 10^{14} cm^{-2}. In previous works, they also pointed out that the interface density of state played a crucial role in the device performance.[49−51] This further reinforces the consideration that there will still be some space to enhance the output characteristics of the device via interface control. Further investigation will be conducted on optimizing the surface passivation to decrease the interface density of the state.

CONCLUSIONS

In summary, we demonstrated the inorganic−organic hybrid silicon solar cells based on SiNWs on a planar silicon substrate and conjugated molecule through solution process. Because of the improvement of light harvesting efficiency and the enhancement of the charge-carrier extraction capability, the cell showed an excellent PCE of 9.70% under AM 1.5 solar spectrum irradiation at 100 mW/cm^2. The presence of SiNWs on a silicon substrate dramatically suppressed the light reflection, which led to the enhancement of the light absorption capability. In addition, the charge collection benefited from the novel top contact scheme with a thin organic layer on both SiNWs and the silicon substrate. Thus, the heterojunction of a thin organic layer on SiNWs structure standing on the planar component took the advantages of both their excellent output characteristics of light harvesting capability and charge extraction efficiency, which increased the J_{sc} as well as the FF. The hybrid device via a simple method would be a potential technological alternative to a crystalline silicon device with diffused p−n junctions.

ASSOCIATED CONTENT

Supporting Information. Absorption spectra of spiro-OMeTAD film and a-Si film, schematic and image of hybrid device with six pixels electrode, EQE measuring area, XPS emission of CH_3−SiNWs, current density−voltage behavior of hybrid device-based hydrogen-terminated silicon surface, current density−voltage behavior of devices 1 and 2 in the dark, and light reflection of SiNWs substrate and polished planar substrate. This material is available free of charge via the Internet at http://pubs.acs.org.

AUTHOR INFORMATION

Corresponding Author
bqsun@suda.edu.cn; apannale@cityu.edu.hk

ACKNOWLEDGMENT

This work was supported by the National Basic Research Program of China (973 Program) (Grant No. 2012CB932402), the National Natural Science Foundation of China (Grant Nos. 60976050, 61176057, 91123005), the Scientific Research Foundation for the Returned Overseas Chinese Scholars of State Education Ministry, the Priority Academic Program Development of Jiangsu Higher Education Institutions, and the Research Grants Council of HKSAR (No. CityU 101909). X.S. would like to thank Innovative Graduate Education Program of Jiangsu (No. CXZZ11_0098).

REFERENCES

(1) Hoffmann, W. *Sol. Energy Mater. Sol. Cells* **2006**, *90*, 3285.
(2) Garnett, E.; Yang, P. *Nano Lett.* **2010**, *10*, 1082.
(3) Boettcher, S. W.; Spurgeon, J. M.; Putnam, M. C.; Warren, E. L.; Turner-Evans, D. B.; Kelzenberg, M. D.; Maiolo, J. R.; Atwater, H. A.; Lewis, N. S. *Science* **2010**, *327*, 185.
(4) Garnett, E. C.; Yang, P. *J. Am. Chem. Soc.* **2008**, *130*, 9224.
(5) Jung, J. Y.; Guo, Z.; Jee, S. W.; Um, H. D.; Park, K. T.; Hyun, M. S.; Yang, J. M.; Lee, J. H. *Nanotechnology* **2010**, *21*, 445303.
(6) Sivakov, V.; Andr, G.; Gawlik, A.; Berger, A.; Plentz, J.; Falk, F.; Christiansen, S. *Nano Lett.* **2009**, *9*, 1549.

(7) Yoon, H. P.; Yuwen, Y. A.; Kendrick, C. E.; Barber, G. D.; Podraza, N. J.; Redwing, J. M.; Mallouk, T. E.; Wronski, C. R.; Mayer, T. S. *Appl. Phys. Lett.* **2010**, *96*, 213503.
(8) Yuan, G.; Zhao, H.; Liu, X.; Hasanali, Z. S.; Zou, Y.; Levine, A.; Wang, D. *Angew. Chem., Int. Ed.* **2009**, *121*, 9860.
(9) Zhu, J.; Yu, Z.; Burkhard, G. F.; Hsu, C. M.; Connor, S. T.; Xu, Y.; Wang, Q.; McGehee, M.; Fan, S.; Cui, Y. *Nano Lett.* **2008**, *9*, 279.
(10) Putnam, M. C.; Boettcher, S. W.; Kelzenberg, M. D.; Turner-Evans, D. B.; Spurgeon, J. M.; Warren, E. L.; Briggs, R. M.; Lewis, N. S.; Atwater, H. A. *Energy Environ. Sci.* **2010**, *3*, 1037.
(11) Peng, K.; Xu, Y.; Wu, Y.; Yan, Y.; Lee, S. T.; Zhu, J. *Small* **2005**, *1*, 1062.
(12) Peng, K. Q.; Wang, X.; Wu, X. L.; Lee, S. T. *Nano Lett.* **2009**, *9*, 3704.
(13) Kelzenberg, M. D.; Boettcher, S. W.; Petykiewicz, J. A.; Turner-Evans, D. B.; Putnam, M. C.; Warren, E. L.; Spurgeon, J. M.; Briggs, R. M.; Lewis, N. S.; Atwater, H. A. *Nat. Mater.* **2010**, *9*, 239.
(14) Kayes, B. M.; Atwater, H. A.; Lewis, N. S. *J. Appl. Phys.* **2005**, *97*, 114302.
(15) Peng, K.; Wang, X.; Li, L.; Wu, X.; Lee, S. *J. Am. Chem. Soc.* **2010**, *132*, 6872.
(16) Gunawan, O.; Wang, K.; Fallahazad, B.; Zhang, Y.; Tutuc, E.; Guha, S. *Prog. Photovoltaics: Res. Appl.* **2011**, *19*, 307.
(17) Peng, K. Q.; Lee, S. T. *Adv. Mater.* **2011**, *23*, 198.
(18) Dan, Y. P.; Seo, K.; Takei, K.; Meza, J. H.; Javey, A.; Crozier, K. B. *Nano Lett.* **2011**, *11*, 2527.
(19) Kim, D. R.; Lee, C. H.; Rao, P. M.; Cho, I. S.; Zheng, X. *Nano Lett.* **2011**, *11*, 2704.
(20) Shiu, S. C.; Chao, J. J.; Hung, S. C.; Yeh, C. L.; Lin, C. F. *Chem. Mater.* **2010**, *22*, 3108.
(21) Garnett, E. C.; Peters, C.; Brongersma, M.; Cui, Y.; McGehee, M. *Photovoltaic Specialists Conference (PVSC), 2010 35th IEEE*; IEEE: HI, 2010; p 000934.
(22) Lin, D. H.; Shiu, S. C.; Huang, J. S.; Lin, C. F. *Photovoltaic Specialists Conference (PVSC), 2010 35th IEEE*; IEEE: HI, 2010; p 000949.
(23) Zhang, F.; Sun, B.; Song, T.; Zhu, X.; Lee, S. *Chem. Mater.* **2011**, *23*, 2084.
(24) Adikaari, A.; Dissanayake, D.; Hatton, R.; Silva, S. *Appl. Phys. Lett.* **2007**, *90*, 203514.
(25) Huang, J. S.; Hsiao, C. Y.; Syu, S. J.; Chao, J. J.; Lin, C. F. *Sol. Energy Mater. Sol. Cells* **2009**, *93*, 621.
(26) Dimitrakopoulos, C. D.; Malenfant, P. R. L. *Adv. Mater.* **2002**, *14*, 99.
(27) Kuo, C. Y.; Gau, C. *Appl. Phys. Lett.* **2009**, *95*, 053302.
(28) Gowrishankar, V.; Scully, S. R.; McGehee, M. D.; Wang, Q.; Branz, H. M. *Appl. Phys. Lett.* **2006**, *89*, 252102.
(29) Alet, P. J.; Palacin, S.; Cabarrocas, P. R. I.; Kalache, B.; Firon, M.; de Bettignies, R. *Eur. Phys. J.: Appl. Phys.* **2006**, *36*, 231.
(30) Haick, H.; Hurley, P. T.; Hochbaum, A. I.; Yang, P.; Lewis, N. S. *J. Am. Chem. Soc.* **2006**, *128*, 8990.
(31) Bansal, A.; Li, X.; Lauermann, I.; Lewis, N. S.; Yi, S. I.; Weinberg, W. H. *J. Am. Chem. Soc.* **1996**, *118*, 7225.
(32) Bashouti, M.; Stelzner, T.; Berger, A.; Christiansen, S.; Haick, H. *J. Phys. Chem. C* **2009**, *113*, 14823.
(33) Bashouti, M. Y.; Paska, Y.; Puniredd, S. R.; Stelzner, T.; Christiansen, S.; Haick, H. *Phys. Chem. Chem. Phys.* **2009**, *11*, 3845.
(34) Bashouti, M. Y.; Stelzner, T.; Berger, A.; Christiansen, S.; Haick, H. *J. Phys. Chem. C* **2008**, *112*, 19168.
(35) Yum, J. H.; Chen, P.; Gratzel, M.; Nazeeruddin, M. K. *ChemSusChem* **2008**, *1*, 699.
(36) Snaith, H. J.; Moule, A. J.; Klein, C.; Meerholz, K.; Friend, R. H.; Gratzel, M. *Nano Lett.* **2007**, *7*, 3372.
(37) Bach, U.; Lupo, D.; Comte, P.; Moser, J.; Weissrtel, F.; Salbeck, J.; Spreitzer, H.; Gratzel, M. *Nature* **1998**, *395*, 583.
(38) Ding, I. K.; Tetreault, N.; Brillet, J.; Hardin, B. E.; Smith, E. H.; Rosenthal, S. J.; Sauvage, F.; Gratzel, M.; McGehee, M. D. *Adv. Funct. Mater.* **2009**, *19*, 2431.
(39) Ding, I. K.; Tetreault, N.; Brillet, J.; Hardin, B. E.; Smith, E. H.; Rosenthal, S. J.; Sauvage, F.; Gratzel, M.; McGehee, M. D. *Adv. Funct. Mater.* **2009**, *19*, 1.
(40) Roman, L. S.; Mammo, W.; Pettersson, L.; Andersson, M.; Inganas, O. *Adv. Mater.* **1998**, *10*, 774.
(41) Zhao, J.; Wang, A.; Green, M. A.; Ferrazza, F. *Appl. Phys. Lett.* **1998**, *73*, 1991.
(42) Shen, X.; Sun, B.; Yan, F.; Zhao, J.; Zhang, F.; Wang, S.; Zhu, X.; Lee, S. *ACS Nano* **2010**, *4*, 5869.
(43) Royea, W. J.; Juang, A.; Lewis, N. S. *Appl. Phys. Lett.* **2000**, *77*, 1988.
(44) Lin, C. H.; Chattopadhyay, S.; Hsu, C. W.; Wu, M. H.; Chen, W. C.; Wu, C. T.; Tseng, S. C.; Hwang, J. S.; Lee, J. H.; Chen, C. W. *Adv. Mater.* **2009**, *21*, 759.
(45) Eades, W. D.; Swanson, R. M. *J. Appl. Phys.* **1985**, *58*, 4267.
(46) Price, M. J.; Foley, J. M.; May, R. A.; Maldonado, S. *Appl. Phys. Lett.* **2010**, *97*, 083503.
(47) Taguchi, M.; Terakawa, A.; Maruyama, E.; Tanaka, M. *Prog. Photovoltaics: Res. Appl.* **2005**, *13*, 481.
(48) Maiolo, J. R., III; Atwater, H. A.; Lewis, N. S. *J. Phys. Chem. C* **2008**, *112*, 6194.
(49) Schmidt, M.; Korte, L.; Laades, A.; Stangl, R.; Schubert, C.; Angermann, H.; Conrad, E.; Maydell, K. *Thin Solid Films* **2007**, *515*, 7475.
(50) Schulze, T.; Beushausen, H.; Leendertz, C.; Dobrich, A.; Rech, B.; Korte, L. *Appl. Phys. Lett.* **2010**, *96*, 252102.
(51) Scharber, M. C.; Muhlbacher, D.; Koppe, M.; Denk, P.; Waldauf, C.; Heeger, A. J.; Brabec, C. J. *Adv. Mater.* **2006**, *18*, 789.